Classification
Physics Abstracts
61.16D — 81.20L

HREM studies of intergrowth between NbO and perovskite in the Ba-, Sr and K-Nb-O systems

Gunnar Svensson

Department of Inorganic Chemistry, Stockholm University, S-106 91 Stockholm, Sweden

(Received October 01, 1990; accepted January 15, 1991)

Résumé. — Des structures d'intercroissance ordonnées et désordonnées entre la perovskite et NbO dans les systèmes Ba-, Sr- et K-NbO ont été étudiées par microscopie électronique et diffraction X sur poudres. Les structures ordonnées KNb_4O_6 et $A(II)_2Nb_5O_9$ (A (I) = K et A (II) = Sr, Ba) consistent en une intercroissance lamellaire de feuillets A (I, II) NbO_3 et NbO, ce dernier ayant une maille d'épaisseur. Dans les systèmes A (II)-Nb-O, une intercroissance bidimensionnelle entre des blocs de différentes tailles de A (I, II) NbO_3 et NbO existe dans un domaine α: la région des phasoïdes. Les études combinées de microscopie haute résolution et de microanalyse X des phasoïdes α ont donné une composition approximative $\sim BaNb_4O_6$. Dans les images haute résolution, de petits domaines d'intercroissances mieux ordonnées ont été reconnus. Ils sont discutés en termes de "microphases" et de séries homologues. Des facteurs influençant la taille des blocs dans la structure sont aussi discutés.

Abstract. — Ordered and disordered intergrowth structures between perovskite and NbO type elements in the K-, Sr- and Ba-Nb-O systems have been studied by means of electron microscopy and X-ray powder diffraction techniques. The ordered structures KNb_4O_6 and $A(II)_2Nb_5O_9$ (A(I)= K and A (II) = Sr, Ba) consist of lamellar intergrowths of A(I, II)NbO_3 and NbO slabs, the latter being one unit cell thick. In the A (II)-Nb-O systems a two dimensional intergrowth between A(I, II)NbO_3 and NbO blocks of varying sizes also exist, in a *phasoid* region called α. Combined HREM studies and EDS-analysis of the Ba-analogue of the α-phasoid gives the approximate composition $\sim BaNb_4O_6$. In the HREM images one can also find small domains of more ordered intergrowth. These are discussed in terms of "micro-phases" and homologous series. Some factors influencing the block sizes in the structure are also discussed.

1. Introduction.

Rather often simple structures can grow together in a regular manner, forming new, so-called "intergrowth structures". When the basic units have different compositions, the intergrowth can in principle attain any intermediate composition by variation of the sizes and accordingly the relative proportions of the two units. If the intergrowth is ordered, such variation gives rise to an unlimited number of different phases, which are members of a general homologous series. Often

the intergrowth contains defects, however, which could be anything from isolated units with deviant sizes to a completely random arrangement of different-sized blocks. This makes the usual concept of "phase" difficult to apply, and Magnéli has suggested the term *phasoid* for the latter cases [1].

In the reduced K-, Sr- and Ba-Nb-O systems there exist ordered intergrowth structures between perovskite and NbO type elements. In the two latter systems phasoid regions have also been found, while in the K–Nb–O system defects frequently occur in the ordered structure. Models of perovskite and NbO are shown in figure 1a. NbO has an ordered deficient NaCl-type structure with 1/4 of both anion and cation sites vacant. It can also be described as a cubic close-packed array of oxygen where 1/4 of the oxygens are replaced by vertex-linked Nb_6 octahedra with Nb-Nb bonds along the edges [2]. The structure has also been pictured as blocks of condensed Nb_6O_{12} clusters [3]. The perovskite parts A(I, II)NbO_3 (A (I) = K [4] and A (II) = Sr [5], Ba [5] are cubic closest packed AO_3 layers with Nb atoms in the octahedral inter-layer cavities formed between the oxygen atoms, see figure 1b. Alternatively, it can be seen as a network of corner-sharing NbO_6 octahedra, with the A atoms enclosed cubo-octahedra formed by the NbO_6 oxygens.

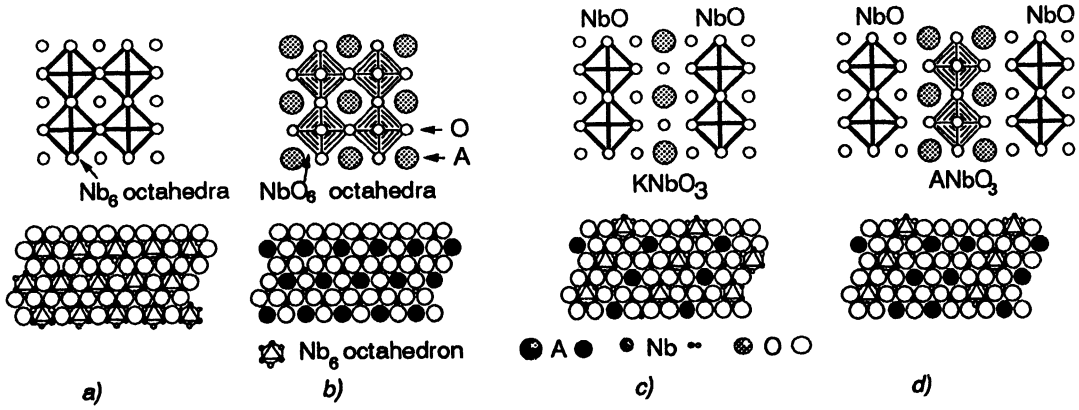

Fig. 1. — a) Model of NbO seen along the a-axis. The Nb_6 octahedron (bold lines) and the oxygen atoms are shown. b) Model of A(I, II)NbO_3 (perovskite type). Below, in a) and b), the structures are viewed along <111>, showing one close-packed layer of oxygen atoms and Nb_6 octahedra or A atoms. c) ~ KNb_4O_6 and d) $A(II)_2Nb_5O_9$ showing the alternating slabs of NbO and perovskite. Below in c) and d) the close-packed layers of K or A(II) and O atoms and Nb_6 octahedra are shown. Note the similarity between the structures of NbO, A(I, II)NbO_3, ~ KNb_4O_6 and $A(II)_2Nb_5O_9$.

The ordered structures of KNb_4O_6 [6] and $A(II)_2Nb_5O_9$ [7, 8] can be described as lamellar intergrowths of A(I, II)NbO_3 and NbO. The NbO slabs are one unit cell thick and the perovskite layer is one unit cell thick in ~ KNb_4O_6 and two units thick in $A(II)_2Nb_5O_9$, with boundary atoms in common, as shown in figure 1. As with A(I, II)NbO_3 and NbO, the structures can be described in terms of close-packed layers of O atoms in ccp arrangement. In these layers 1/4 or of oxygen atoms are replaced by A atoms of Nb_6 octahedra.

The close relation between the unit cells of KNb_4O_6 $A(II)_2Nb_5O_9$, NbO and A(I, II)NbO_3 has been discussed elsewhere [6, 9] and will therefore only be briefly touched upon below. The above mentioned systems have been studied by means of X-ray powder diffraction and electron microscope techniques. This paper will mainly deal with the Ba–Nb–O system, but the K and Sr analogues will to some extent also be discussed.

2. Experimental.

Appropriate amounts of $A(II)_5Nb_4O_{15}$, or $KNbO_3$, Nb and Nb_2O_5 were ground and pelleted in order to minimise the reaction with the evacuated silica reaction tube. Temperatures between 1000 °C and 1250 °C (950–1100 °C for the K analogues [6]) were used. For the Ba system several types of quenching schemes have been compared: air- and water-quenching, and slow cooling (5 °C/h). After heating, the pellets have a crust of silicon-containing products. These surface products were removed mechanically, and the inner silicon-free parts were used.

X-ray powder diffraction patterns were recorded in a focusing camera of Guinier-Hägg type, using Cu $K\alpha_1$ radiation, and silicon [10] was added as internal standard. The photographs were analysed with a film-scanner system [11].

Electron microscopy studies were made at 200 kV in JEOL JEM-200CX and JEOL JEM-2000FX microscopes. Small amounts of the samples chosen for study in the microscopes were crushed in an agate mortar and dispersed in *n*-butanol. A drop of this dispersion was put on a holey carbon-film coated Cu-grid. High-resolution electron micrographs were taken in the JEOL JEM-200CX microscope having a top-entry goniometer (± 10°). The point-to-point resolution is 2.4 Å. The compositions of individual crystal fragments were determined in the JEOL JEM-2000FX electron microscope with an attached energy-dispersive analysing system.

Structure models obtained from the electron micrographs were checked by image calculations according to the multislice method, using the SHRLI [12] suite of computer programs.

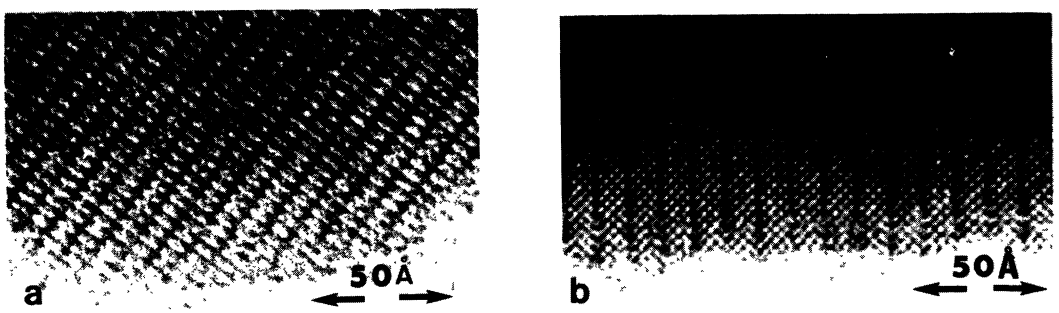

Fig. 2. — HREM image of a) ~ KNb_4O_6 and b) $Ba_2Nb_5O_9$ along <100>. Dark lamella of NbO interleaved by a square lattice of dark spots corresponding to a) K and b) Ba and Nb atoms respectively.

3. X-ray powder diffraction in the Ba-Nb-O system.

In 1989, Svensson [13] reported that a relative intensity change of the X-ray diffraction lines corresponding to $Ba_2Nb_5O_9$ was observed when the compositions of the samples were moved from $Ba_2Nb_5O_9$ towards the NbO-Nb_2O_5 binary line. The hkl $l \neq 0$ reflections from $Ba_2Nb_5O_9$ decreased in intensity while those at $\sin^2\theta$ positions corresponding $hk0$ increased in intensity. The position of $hk0$ lines shifted slightly with composition. This continued to a point where the first type of reflections disappeared and only $hk0$ lines remained. These remaining reflections together with some new ones could be indexed with a C-centered tetragonal subcell: see table I below. (The

choice of a C-centered tetragonal cell is non-standard but is convenient here). The corresponding "phase", or rather *phasoid*, was called α. A sample with the nominal composition $BaNb_4O_6$, heated at 1200 °C and air quenched yielded a nearly monophasic sample after several regrindings. The powder pattern showed lines from a and some very faint lines corresponding to NbO and $Ba_3Nb_{21-x}Si_2O_{44}$ [14]. The source of silicon was the reaction tube wall. At lower synthesis temperatures, (1120 °C) reflections from NbO or other phases were always present in the powder patterns.

4. HREM studies.

In HREM images of the intergrowth phases between $A(I,II)NbO_3$ (A(I)= K, A(II)= Sr, Ba) and NbO only the heavier metal atoms can be expected to give significant contrast. HREM images of stoichiometric $Ba_2Nb_5O_9$ and ~ KNb_4O_6 are shown in figure 2. As seen, the NbO part forms slabs, one Nb_6 octahedron thick, interleaved by slabs of perovskite of a thickness of two units and one unit, respectively. The metal-dense NbO layers appear in the images with dark contrast, and the metal atoms in the perovskite are revealed as a square net of dots. These dots correspond to strings, parallel to the line of sight, of Nb + O and Ba in $Ba_2Nb_5O_9$, and of K in ~ KNb_4O_6. For $Ba_2Nb_5O_9$ the sums of atomic numbers, $\sum Z$, of Ba and of Nb + O at these two projected sites are rather similar. The difference in scattering power is thus not large enough to be seen in the images.

As for all intergrowth structures, a whole family of phases can be imagined in which the various members differ only with respect to the width of the two structure elements. In the present system the composition of these one-dimensional intergrowth phases would fall on various points along the $A(I,II)NbO_3$-NbO line in the phase diagram. In these structures there is also an inherent tendency to form defects and disorder. In the K-, Sr- and Ba-Nb-O systems, several types of disorder have been found, which can essentially be divided into two groups, corresponding to one- and two-dimensional intergrowth.

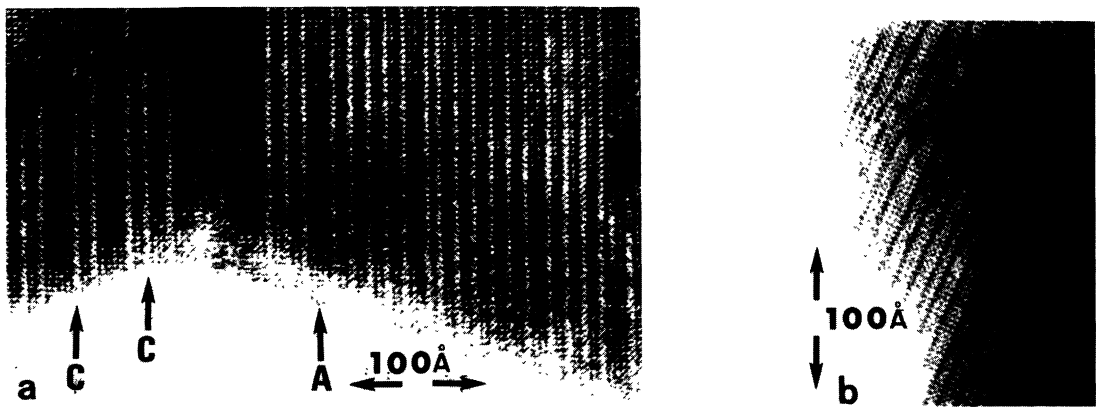

Fig. 3. — HREM images showing examples of variation in the NbO and perovskite slab widths. a) A crystal found in a sample with gross composition $BaNb_5O_8$, showing disordered intergrowth of BaO and NbO. The BaO layers can be considered as a slice of the perovskite type $BaNbO_3$, similar to those in ~ KNb_4O_6. b) Defects found in $Sr_2Nb_5O_9$, both missing ($n = 1$) and extra ($n = 3$) perovskite slabs can be seen.

4.1 ONE-DIMENSIONAL DISORDER. — HREM images with one-dimensionally disordered intergrowth in the Ba and the Sr-Nb-O systems are shown in figure 3. The structure in a) can be described as consisting of alternating layers of BaO and NbO. The width of the layers varies. Layers up to 6 Nb_6 octahedra wide are readily seen in the image. Some NbO (A) and BaO (C) slabs are marked in the image. The BaO layers can alternatively be described as perovskite layers of minimum width having all their niobium atoms shared with the NbO layers as in $\sim KNb_4O_6$. Variation in the width of the perovskite layer has also been observed, but seems to occur mostly as isolated events. However, it occurs rather frequently in $\sim KNb_4O_6$ [6] and has been found in $Sr_2Nb_5O_9$ [8]. Figure 3b shows such defects in $Sr_2Nb_5O_9$.

4.2 TWO-DIMENSIONAL DISORDER. — A typical HREM image of α is shown in figure 4. The thin parts of the crystal shown are seen to consist of a 2.9 Å square lattice of dark spots with rows and blocks of larger spots or crosses. Image simulations verify that these spots correspond to the Nb_6 octahedra in Nb_6O_{12} clusters [13], and the blocks can thus be seen as units of NbO. At least in the thin parts these blocks continue through the crystal as columns. As evident in the image, the size of the NbO blocks varies. Within the same crystal, single octahedral columns have been found, as well as larger blocks consisting of more than 30 corner-sharing Nb_6 octahedra in projection. The square net between the NbO blocks corresponds to the Ba and Nb atoms in the perovskite type framework.

4.3 INTERPRETATIONS OF THE HREM IMAGES. — When inserting an isolated NbO block into a perovskite type structure as shown in figure 5, two sides of the block marked A have the same orientation relative to the perovskite part as found in $Ba_2Nb_5O_9$. The boundary Nb atoms in the NbO block are connected to the perovskite parts so that straight Nb-O-Nb bonds form. The Nb_6 and NbO_6 octahedra are thus lined up in this direction. Across the other edges (B) the boundary Nb atoms are connected as in edge-sharing octahedra, and the rows of Nb_6 and NbO_6 octahedra are shifted relative to each other.

In the interpretation of the HREM images, the structures have been assumed to continue through the crystal in the viewing direction in the thin parts of the crystallites, with all atomic positions fully occupied.

The size of the rectangular NbO blocks will be indicated as n^*m where n and m are numbers of NbO_6 octahedra. The size of the perovskite block is p^*q, p and q being the block size in terms of NbO_6 octahedra not sharing boundary atoms with the NbO blocks.

As was mentioned above, the difference in contrast between barium and niobium is very small at the defocus used. It is thus practically impossible to say how the NbO blocks are oriented relative to the perovskite blocks in the HREM images. Essentially two models are possible. i) The perovskite parts are assumed to be coherent throughout the crystals, and the NbO columns/blocks to be inserted in an already existing perovskite lattice (Fig. 5). ii) The perovskite blocks between the NbO blocks are independently oriented so as to maximise the amount of Ba. This is illustrated in figure 6, where the two alternative models (b and c) are used to interpret the area enclosed in the image. The first model assumes a coherent perovskite lattice, but in the images this is not observed. The crystal shown can be described as a two-dimensional intergrowth between NbO and $BaNbO_3$ blocks. But the interpreted area can equally well be described in terms of fault lines in $Ba_2Nb_5O_9$. At each arrow the structure is sheared by the vector [1/2a 0 1/2c] along {100} in $Ba_2Nb_5O_9$, (including the perovskite net). In areas having blocks of more random sizes and relative positions, a tendency for each NbO block to connect with four neighbouring ones *via* a shared oxygen atom can be seen. Such a linking is marked with an arrow in figure 6b. This linking gives each NbO block four independent perovskite blocks as neighbours. These perovskite blocks can thus be oriented out of phase with each other, as in model ii) above. If each of the

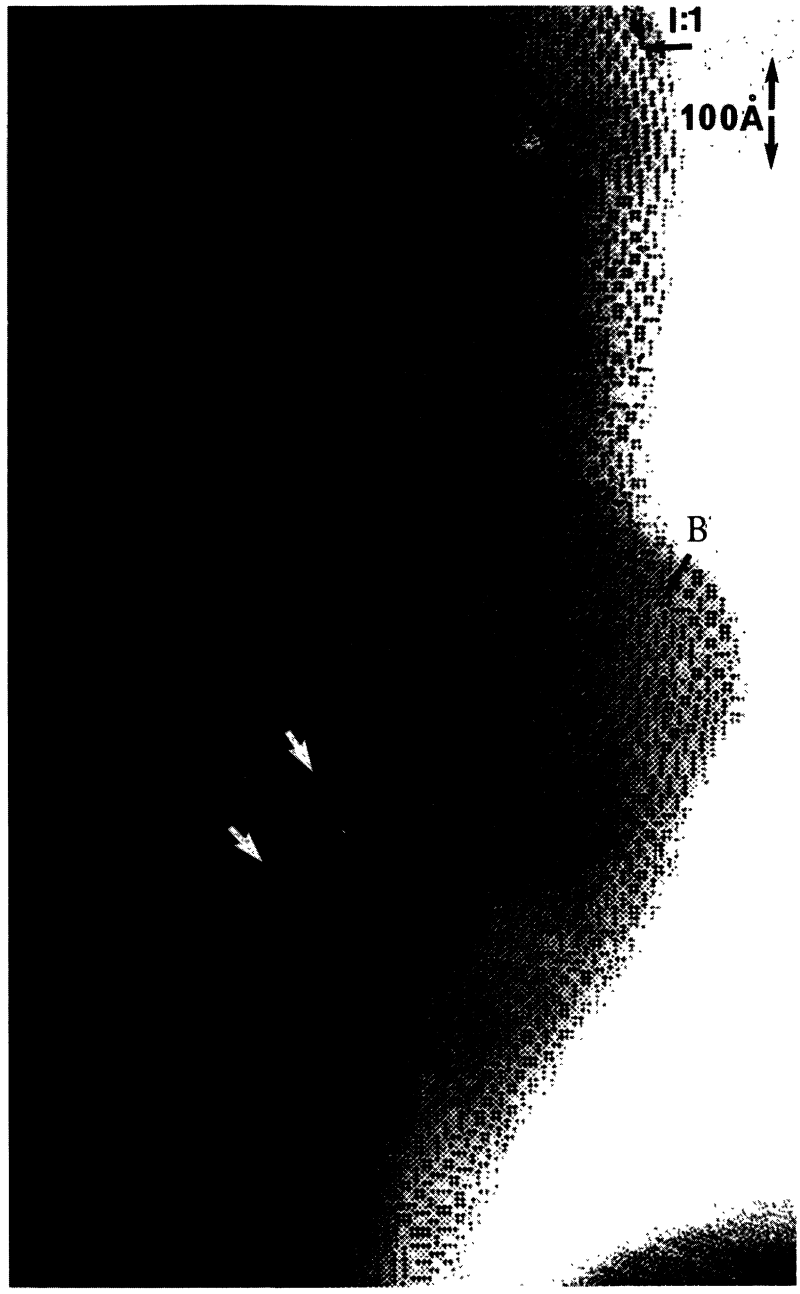

Fig. 4. — Typical HREM image of the α-phasoid. The crystal shown was found in a sample with the gross composition $BaNb_6O_8$. An enlargement of the area marked B is discussed in figure 6. I:1 is an example of homologous phase, see figure 8. The arrows indicate concentration strings, see text.

perovskite blocks is oriented so as to maximise the number of barium atoms within the block, all the boundaries between perovskite and NbO will be of the type found in $Ba_2Nb_5O_9$. This is clearly different from the situation in figure 6c, where the NbO blocks have two different types of boundary to the perovskite matrices, A and B.

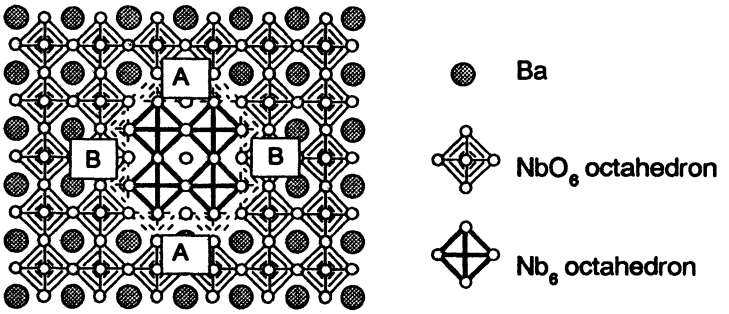

Fig. 5. — Model of an NbO block inserted in a $BaNbO_3$ matrix. Special NbO_6 octahedra, with Nb atoms, that are boundary atoms between the perovskite matrix and the NbO block, are shown with broken lines. The two sides of the block marked A have the same orientations toward the perovskite parts as in ~ KNb_4O_6 and Nb_6 and NbO_6 octahedra are thus lined up in this direction. Across the other edges, B, the Nb_6 and NbO_6 octahedral rows are shifted relative to each other.

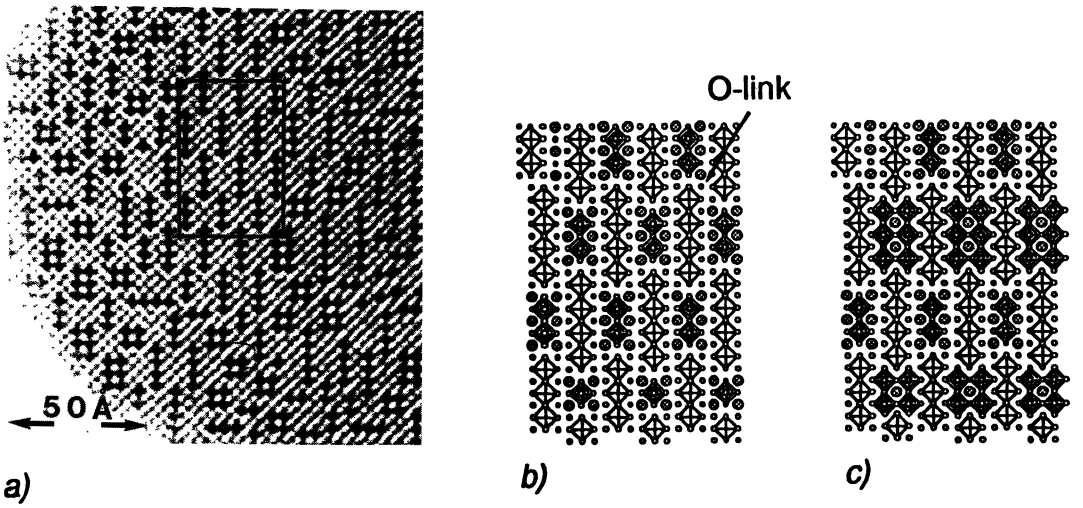

Fig. 6. — a) An enlargement of the area marked B in figure 4. b) and c) are two different interpretations of the enclosed area. In b) the perovskite matrix between the NbO blocks is assumed to be coherent. In c) the perovskite blocks between the NbO blocks are independently oriented so as to maximise the amount of Ba. The models give a Nb/Ba ratio of 3.4 for b) and 5.2 for c). A part of the region interpreted can be described in terms of fault lines in $Ba_2Nb_5O_9$. At each arrow the structure is sheared by the vector [1/2a, 0, 1/2c] along {100} in $Ba_2Nb_5O_9$. In b) an oxygen shared between two NbO blocks is marked.

For the area shown in figure 6b and c, the two models give Nb/Ba $\approx$ 3.4 and 5.2, respectively. EDS-analysis of individual fragments of the α phasoid indicated a Nb/Ba ratio of 3.2-4.5 (unpublished results). Several samples where analysed but no correlation between initial composition and the observed composition of α was found. The analysis thus gives support to the model of figure 6b.

4.4 $BaNbO_3$-RICH INTERGROWTH. — An example of $BaNbO_3$-rich intergrowth is shown in figure 7. A large part of the crystal, marked A, seems to be $BaNbO_3$, and the other part (B) to be $Ba_2Nb_5O_9$. At the boundary between A and B there are three fault line where the $Ba_2Nb_5O_9$ structure is sheared along the *c*-axis, as discussed above. Between the shifts there are 9*1 and 4*1 NbO blocks. Note that one of the 9*1 NbO block is missing, except for one isolated Nb_6 octahedron at each end. These Nb_6 octahedra separate the perovskite sublattice on different sides of the fault lines, thereby making it possible to orient then independently as discussed above. A model of this area is shown in figure 7.

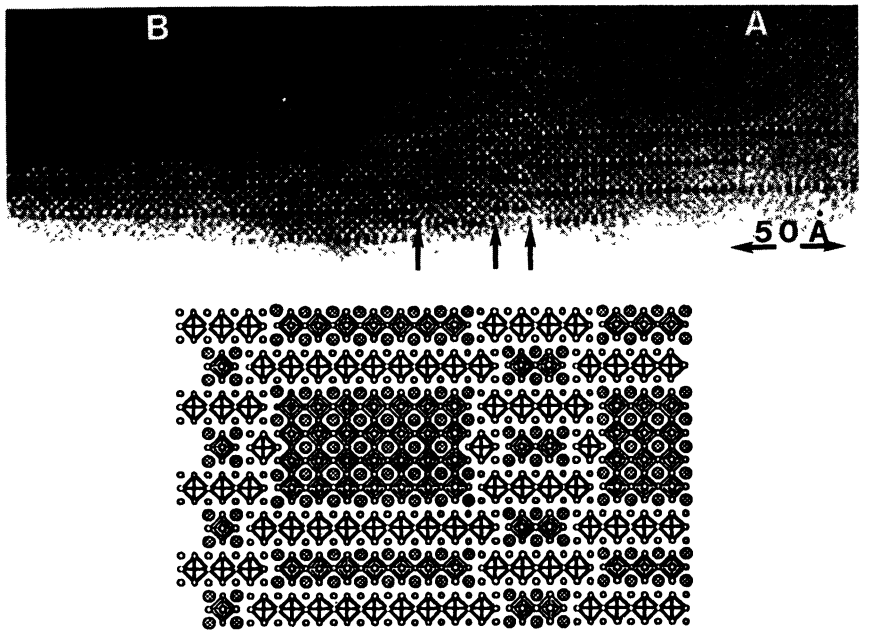

Fig. 7. — a) HREM image of a crystal from a sample of composition $BaNb_2O_4$. A large part of the crystal, (marked A) is $BaNbO_3$ and the other part (B) is $Ba_2Nb_5O_9$. At the boundary three fault lines are arrowed. b) A tentative interpretation of the boundary marked in a). Between the arrowed fault lines there are 9*1 and 4*1 NbO blocks. Note that one of the 9*1 NbO blocks is missing, except for one single Nb_6 octahedron at each end. These octahedra separate the perovskite blocks on different sides of the fault lines thereby making it possible for them to be shifted out of phase.

It was mentioned above that the NbO blocks are normally linked to 4 neighbouring NbO blocks *via* shared oxygen atoms. According to the interpretations of the disordered intergrowth presented above, this linkage should give relatively short Nb-Nb distances ($\sim$ 2.9 Å) between different NbO blocks. There could thus be metal-metal bonds between Nb_6O_{12} clusters in neighbouring blocks. However, since the exact interatomic distances are unknown, this remains unconfirmed. Other types of linking have been observed, for example edge-sharing of Nb_6 octahedra.

The sizes of the NbO-blocks vary widely, but the most common sizes seem to be 3*1, 2*2 and 3*2 Nb_6 octahedra. The size of the perovskite blocks is frequently p*1 NbO_6 octahedra with $p = 1$ or 2. In one direction this gives an NbO a block separation equal to that in $Ba_2Nb_5O_9$. No significant variation in block size distribution has so far been found in samples of α with different compositions. The shape of the blocks is normally rectangular, but other more complex shapes have also been observed.

5. Homologous phases.

In many of the HREM images, domains of ordered structure are seen. Such an area is delineated as I:1 in figure 4. These domains can be interpreted in terms of "micro-phases". Although the ordered domains are quite small, their identification helps to systematise the quasi-ordered intergrowth between $ANbO_3$ and NbO. It can also give a better understanding of the compositional variations within the crystals.

5.1 HOMOLOGOUS SERIES. — In figure 8a summary is presented of some of the infinitely many microphases that can conceivably be formed by intergrowth of perovskite-and NbO-type blocks. They can be considered as members of different homologous series. Only a few of the members are listed, many of which have been recognized in HREM images (i.e. at least one unit cell found). The following selection rules have been applied to the two-dimensional series: i) no mixed-size-block phases are considered, ii) the linking scheme between the NbO blocks is limited to a shared oxygen atom, iii) each block is linked to four neighbouring NbO-blocks in this way. It is assumed that the structures are simple along the line of sight so that the repeat unit in this direction comprises the height of one polyhedron only.

Five different homologous series have been considered, differing with respect to the sizes and relative orientations of the NbO and perovskite-type. Series I-IV have rectangular blocks limited in two dimensions, except the end members with $z = \infty$, which have lamellar structures. These end members all belong to a separate one-dimensional series, which is designated Series 0 here. Their composition all fall on the binary $ANbO_3$-NbO line.

Series 0, w*$ANbO_3$ – 3*z*NbO (or more generally $A_wNb_{w+3z}O_{3w+3z}$). This Series is a one-dimensional intergrowth between w*$ANbO_3$ – 3*z*NbO. The stoichiometric $Ba_2Nb_5O_9$($w = 2$, $z = 1$) has been found. In figure 3, members with varying NbO width, $1 \leq z \leq 6$ and $w = 1$, are shown. Stoichiometric members have also been found for K (KNb_4O_6 $w = 1$, $z = 1$) and Sr ($Sr_2Nb_5O_9$ $w = 2$, $z = 1$) analogues. In these systems variations in the perovskite layer have been observed rather frequently.

Series I, $A_2Nb_9O_{14}$ – z*$A_2Nb_5O_9$. The members contain single NbO slabs of type $n = 1$. The structure can also be described, starting from $A_2Nb_5O_9$ ($z = \infty$) with {100} fault planes where the lattice is shifted by 1/2**a** + 1/2**c**. The spacing of these fault planes decreases with decreasing z. In principle all the members shown have been found as defects; the most frequently occuring being the one with $z = 1$. In many micrographs "large" domains are found, as shown in figure 4. For Series II-IV see figure 8 and reference [9].

Several attempts to synthesise these microphases or at least to produce less disordered phases, have been made. As examples, slow heating (5 °C/h), water quenching, slow cooling (5 °C/h), temperature cycling at high temperatures (1000 °C-1200 °C), repeated regrinding and reheating have been tried, but without producing more ordered structures, according to the HREM images.

When the domains of microphases are large, they very often seem to be separated by strings of blocks having different sizes. Naturally, such a string will have a composition that differs from that of its surroundings, and often a number of strings can be connected to each other so as to form concentration gradients in a crystal. In figure 4, two such strings are arrowed.

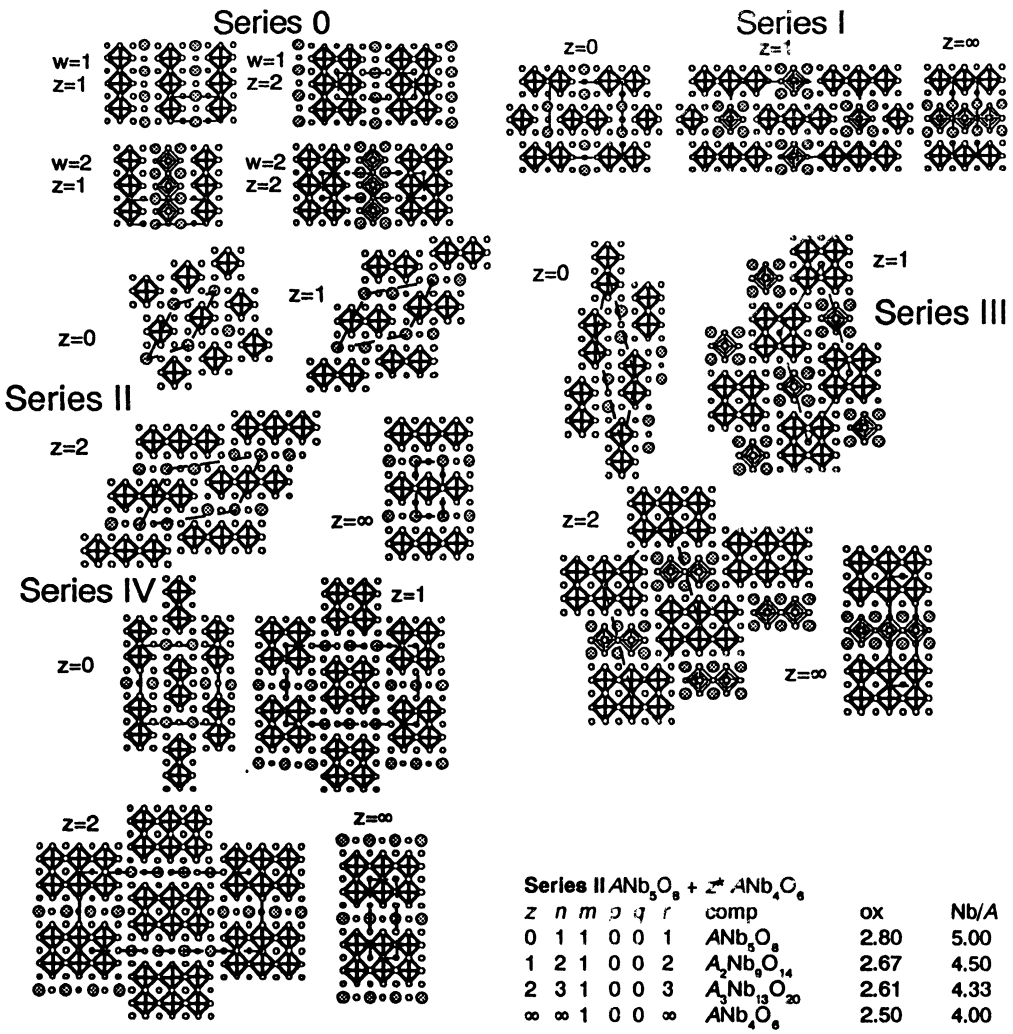

Series 0 Phases on the $ANbO_3$ - NbO binary line.
$w*ANbO_3 + 3*z*NbO$

w	z	comp	ox	Nb/A
1	1	ANb_4O_6	2.50	4.00
1	2	ANb_7O_9	2.29	7.00
2	1	$A_2Nb_5O_9$	2.80	2.50
2	2	$A_2Nb_8O_{13}$	2.50	4.00

Series I $A_2Nb_9O_{14} + z^* A_2Nb_5O_9$

z	n	m	p	q	r	comp	ox	Nb/A
0	2	1	0	0	2	$A_2Nb_9O_{14}$	2.67	4.50
1	3	1	1	1	4	$A_4Nb_{14}O_{23}$	2.71	3.50
2	4	1	2	1	6	$A_6Nb_{19}O_{32}$	2.74	3.17
∞	∞	1	∞	1	∞	$A_2Nb_5O_9$	2.80	2.50

Series II $ANb_5O_8 + z^* ANb_4O_6$

z	n	m	p	q	r	comp	ox	Nb/A
0	1	1	0	0	1	ANb_5O_8	2.80	5.00
1	2	1	0	0	2	$A_2Nb_9O_{14}$	2.67	4.50
2	3	1	0	0	3	$A_3Nb_{13}O_{20}$	2.61	4.33
∞	∞	1	0	0	∞	ANb_4O_6	2.50	4.00

Series III $A_2Nb_9O_{14} + z^* A_2Nb_8O_{12}$

z	n	m	p	q	r	comp	ox	Nb/A
0	1	2	0	0	2	$A_2Nb_9O_{14}$	2.67	4.50
1	2	2	1	1	4	$A_4Nb_{17}O_{26}$	2.59	4.25
2	3	2	2	1	6	$A_6Nb_{25}O_{38}$	2.56	4.17
∞	∞	2	∞	1	∞	$A_2Nb_8O_{12}$	2.50	4.00

Series IV $A_2Nb_9O_{14} + z^* ANb_7O_9$

z	n	m	p	q	r	comp	ox	
0	1	2	0	0	2	$A_2Nb_9O_{14}$	2.67	4.50
1	2	2	0	0	3	$A_3Nb_{16}O_{23}$	2.50	5.33
2	3	2	0	0	4	$A_4Nb_{23}O_{32}$	2.44	5.75
∞	∞	2	0	0	∞	ANb_7O_9	2.29	7.00

Fig. 8. — Homologous Series. The NbO blocks are rectangular and linked *via* oxygen atoms. The $ANbO_3$-blocks are rectangular. Only one block size of each is assumed within each series. r = number of A atoms, p = number of NbO_6 octahedra, (rows), q = number of NbO_6 octahedra, (columns), n = number of Nb_6 octahedra, (rows), m = number of Nb_6 octahedra, (columns). comp = composition, ox = average oxidation state.

5.2 COMPOSITIONAL REGION OF α. — The various homologous series of micro-phases discussed above represent a number of inter-growth types recognised in the α phasoid. The composition of all members of these series (except one) are within a narrow triangle on the oxidised side of the $Ba_2Nb_5O_9$-NbO line in the phase diagram. The triangle is defined by the points $Ba_2Nb_5O_9$, $BaNb_7O_9$ and $Ba_2Nb_9O_{14}$, and it may thus represent structural limits of the α phasoid range. The fact that no α is seen in samples of compositions on the left side of the $Ba_2Nb_5O_9$-NbO line is in accordance with these limits. The composition triangle discussed is in good agreement with the EDS results mentioned above and with the phase analysis (1200 °C).

6. Electron diffraction.

An electron diffraction (ED) pattern ($[001]_{sub}$) typical for the α phasoid is shown in figure 9. This type of ED patterns were frequently observed in α-containing samples. The pattern shows a tetragonal subcell with diffuse satellite reflections around the subcell spots. The subcell agrees with the one derived from the X-ray patterns. As mentioned, above the α pattern could be indexed with a C-centered tetragonal subcell, (see Tab. I). Similar ED-patterns have been found in the Sr-Nb-O system [8].

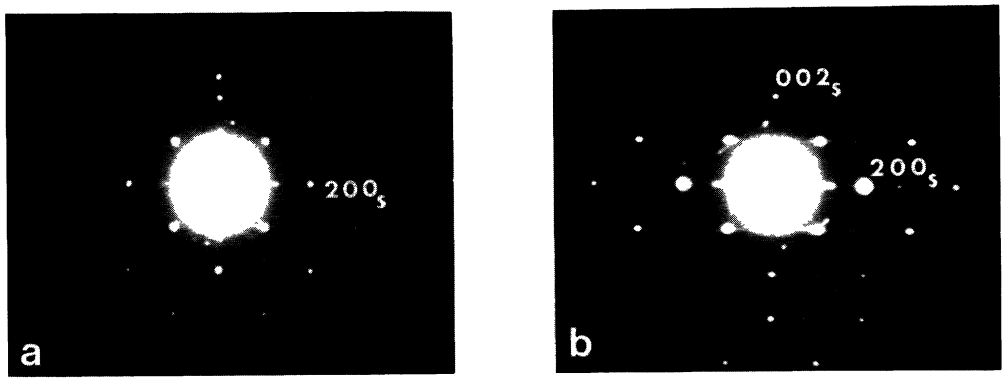

Fig. 9. — a) A typical electron diffraction pattern of α, indicating a C-centered tetragonal subcell with a = 4.1 Å. One sublattice spot is indexed. Around the subcell reflections diffuse satellite spots are seen in two different directions depending on $(h + k)_{sub}$ being even or odd. b) ED pattern of the same crystal as in a), but along $[001]_{sub}$. Note that there is streaking along one direction, indicating a structure disordered in this direction.

The tetragonality of the subcell obtained from X-ray powder patterns indicates the disordered intergrowth of $BaNbO_3$ and NbO, to be two-dimensional. The ED pattern along $[100]_{sub}$, shown in figure 9b, is in accordance with this description. It was obtained from the same crystal as in figure 9a, after tilting. It indicates a subcell of $\sim$ 4.1 Å, but the difference in length of the a and c-axes of α is too small to be distinguished in an ED pattern. There is no streaking along the c^* axis, indicating that there is no disorder along this direction. According to this, a correct description of the α phasoid structure should be a two-dimensional intergrowth of $BaNbO_3$ and NbO columns, even in the thick regions. The C-centering of the substructure is caused by the "out-of-phase" relation between the neighbouring perovskite (and also NbO) blocks. This will

average the scattering power on the Ba and Nb + O positions in the projected structure so as to extinguish the $h + k \neq 2n$ reflections completely.

The satellite reflections in figure 9a form a characteristic pattern. These satellite spots reflect the relative positions and orientations of the NbO blocks. All the satellites around present subreflections are located approximately along the $[110]_{sub}$. In the images it is seen that the connection scheme for the NbO blocks very often is such that wavy "planes" or "chains" are formed. The relative orientations and separations of the planes vary through the crystal, but locally their average direction is somewhere between $\{210\}_{sub}$ and $\{110\}_{sub}$. However, since the planes are not exactly parallel to $[110]_{sub}$, the resulting net will be non-tetragonal ($[100]_{sub} \neq [010]_{sub}$). If the crystal consists of one single domain, then the position of the satellite spots will be different along $[100]_{sub}$ and $[010]_{sub}$. This is indeed observed in some diffraction patterns, where the satellite spots around the $h + k \neq 2n$ and $h + k = 2n$ reflections are non-degenerate, with respect to the $[100]_{sub}$ and $[010]_{sub}$ directions. However, most crystals have domains with similar "chain" orientations, rotated through 90° relative to each other. The positions of the satellite spots then become degenerate and no orientation dependence is observed [9].

7. Discussion.

When discussing these intergrowth phases one should have in mind that both $ANbO_3$ and NbO can be derived from deficient NaCl type structures, where the A, O and the Nb_6 octahedra form cubic close-packed layers. This feature, together with the small size difference between the perovskite and NbO units, could be the simple explanation for the formation of the intergrowth. In table I, some unit cell parameters of interest are given. When $BaNbO_3$ and NbO condense to form $Ba_2Nb_5O_9$, the corner-to-corner (O-Nb-O) distance of the NbO_6 octahedra in $BaNbO_3$ expands from 4.08 Å to 4.16 Å along the a-axis, while it shrinks to 3.86 Å along the c-axis [7, 9]. The latter is probably a compensation for the forced elongation along the a-axis. The Ba-Ba distance along the c-axis is 4.09 Å, which is close to that found in $BaNbO_3$ (4.08 Å), despite the shrinkage of the structure in this direction ; this is probably due to repulsion between the Ba atoms. The overall result is a shorter c-axis than for the corresponding multiple cell of $BaNbO_3$. This is also observed for $Sr_2Nb_5O_9$, and it seems likely that the same distortion of the NbO_6 octahedra is present.

As mentioned above, the perovskite parts between the NbO blocks are generally rather small. The most common perovskite block sizes are the p*1 slabs, where $p = 1$ is very frequent. The stability of these single NbO_6 slabs could be due to the fact that the size difference between the perovskite part and the NbO part can be largely compensated for in a similar way as in $Ba_2Nb_5O_9$. Here, only of the Nb-O bond lengths in the NbO_6 octahedra are fixed by the Nb_6 octahedra in the NbO block (Fig. 10).

The remaining 4 equatorial Nb-O bonds are free to shrink, compensating for the elongation as in $BaNb_5O_9$. In perovskite blocks of the 2^*p, $p \geq 2$ type, figure 10, Ba-Ba repulsion prevents the NbO_6 octahedra from shrinking freely. Only the Nb-O bonds to oxygen atoms shared with the NbO blocks can relax. This could be one reason for the apparent size limitations imposed on both perovskite and NbO block sizes, since these sizes are correlated by geometrical restrictions.

As discussed above, there seems to be only a limited amount of defects along the c-axis of α. One reason for this is that if the perovskite blocks are oriented so as to give A-type boundary to the NbO blocks, then all defects along the c-axis must be of B-type and thus probably unfavourable.

A reason why there is only a single perovskite unit between the NbO slabs in $\sim KNb_4O_6$, instead of two as in $Ba_2Nb_5O_9$ and $Sr_2Nb_5O_9$ could be the decrease in valence electron concentration when going from A^{2+} to A^+.

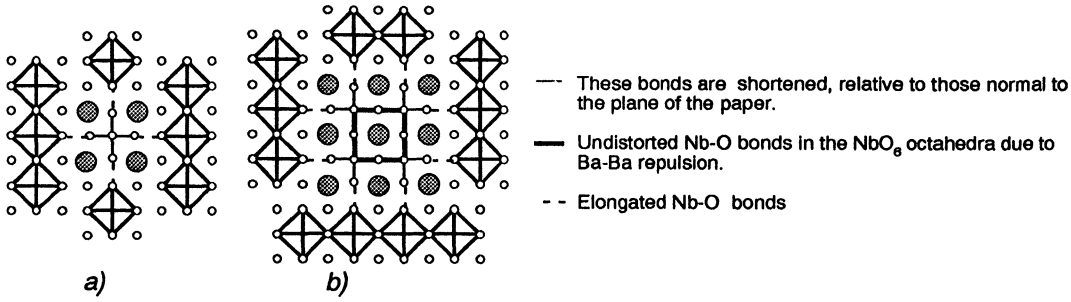

Fig. 10. — a) Model showing a distorted NbO_6 octahedron between four NbO blocks. The Nb-O bonds along the c_{sub} axis are dilated to match the dimension of the NbO blocks, which have been slightly compressed compared to NbO. To compensate for this, the equatorial Ba-O bonds are shortened. b) Model showing a 2*2 perovskite block. Here the A-A repulsions prevent a full distortion of the NbO_6 octahedra, and thereby make larger perovskite blocks less favourable.

Table I. — *Unit cell parameters* (Å) *for* Sr_xNbO_3[5], $BaNbO_3$[5], $KNbO_3$[4], $Ba_2Nb_5O_9$ [7], $Sr_2Nb_5O_9$ [8], ~ KNb_4O_6 [6], NbO [2] Ba *and* Sr *analogues of* α [9, 8].

	$BaNbO_3$	Sr_xNbO_3	$KNbO_3$	NbO	
$a =$	4.085-4.095	3.985-4.025	$5.697\left(\sqrt{2} * 4.028\right)$	4.210	
$b =$			3.971		
$c =$			$5.720\left(\sqrt{2} * 4.045\right)$		
	$Ba_2Nb_5O_9$	$Sr_2Nb_5O_9$	~ KNb_4O_6	Ba α- *phasoid*	Sr α- *phasoid*
$a =$	4.1696	4.1405	4.1393	4.153	4.120
$c =$	12.228	12.040	8.2537	4.157	4.141
	(3*4.076)	(3*4.013)	(2*4.127)		

Acknowledgements.

I wish to thank Professor Lars Kihlborg for many simulations discussions. This work is a part of a research project supported by the Swedish Natural Science Research Council.

References

[1] MAGNÉLI A., *Chem. Scr.* **26** (1986) 535.
[2] BRAUER G., *Z. Anorg. Chem.* **248** (1941) 1.
[3] SCHÄFER H., SCHNERING H. G., *Angew Chem.* **76** (1964) 833.
[4] KATZ L., MEGAW H. D., *Acta Crystallogr.* **22** (1967) 639.
[5] RIDLEY D., WARD R., *J. Am. Chem. Soc.* **77** (1955) 6132.
[6] SVENSSON G., *J. Solid State Chem.* **90** (1991) 249.
[7] SVENSSON G., *Mat. Res. Bull.* **23** (1988) 437.
[8] SVENSSON G., *Acta Chem. Scand.* **44** (1990) 222.
[9] SVENSSON G., *Chem. Commun. Univ. Stockholm* **3** (1989).
[10] HUBBARD C. R., SWANSON H. E., MAUER F. A., *J. Appl. Crystallogr.* **8** (1975) 45.

[11] JOHANSSON K.-E., PALM T., WERNER P.-E., *J. Phys.* **E13** (1980) 128.
[12] O'KEEFE M. A., In: J. J. Hren, F. A. Lenz, E. Munro and P. B. Sewer, Eds., Electron Optical System for Microscopy, Microanalysis and Microlithography, (Proc. 3 rd Pfefferkorn Conf.) SEM Inc., AMF O'Hare, IL 60666, U.S.A. (1984).
[13] SVENSSON G., *Solid State Ionics* **32/33** (1989) 126.
[14] EVANS D. M., KATZ L., *J. Solid State Chem.* **6** (1973) 459.
[15] SVENSSON G., WERNER P.-E., *Mat. Res. Bull.* **25** (1990) 9.